Inorganic Chemistry

Article

pubs.acs.org/IC

# Topotactic Oxidation Pathway of $ScTiO_3$ and High-Temperature Structure Evolution of $ScTiO_{3.5}$ and $Sc_4Ti_3O_{12}$-Type Phases‖

Shahid P. Shafi,[†] Bradley C. Hernden,[†] Lachlan M. D. Cranswick,[‡] Thomas C. Hansen,[§] and Mario Bieringer*,[†]

[†]Department of Chemistry, University of Manitoba, Winnipeg, Manitoba, Canada, R3T 2N2

[‡]Canadian Neutron Beam Centre, National Research Council Canada, Chalk River Laboratories, Chalk River, Ontario, Canada, K0J 1J0

[§]Institut Laue Langevine, 6 rue Jules Horowitz, BP 156, 38042 Grenoble Cedex 9, France

Supporting Information

**ABSTRACT:** The novel oxide defect fluorite phase $ScTiO_{3.5}$ is formed during the topotactic oxidation of $ScTiO_3$ bixbyite. We report the oxidation pathway of $ScTiO_3$ and structure evolution of $ScTiO_{3.5}$, $Sc_4Ti_3O_{12}$, and related scandium-deficient phases as well as high-temperature phase transitions between room temperature and 1300 °C using in-situ X-ray diffraction. We provide the first detailed powder neutron diffraction study for $ScTiO_3$. $ScTiO_3$ crystallizes in the cubic bixbyite structure in space group $Ia\bar{3}$ (206) with $a$ = 9.7099(4) Å. The topotactic oxidation product $ScTiO_{3.5}$ crystallizes in an oxide defect fluorite structure in space group $Fm\bar{3}m$ (225) with $a$ = 4.89199(5) Å. Thermogravimetric and differential thermal analysis experiments combined with in-situ X-ray powder diffraction studies illustrate a complex sequence of a topotactic oxidation pathway, phase segregation, and ion ordering at high temperatures. The optimized bulk synthesis for phase pure $ScTiO_{3.5}$ is presented. In contrast to the vanadium-based defect fluorite phases $AVO_{3.5+x}$ (A = Sc, In) the novel titanium analogue $ScTiO_{3.5}$ is stable over a wide temperature range. Above 950 °C $ScTiO_{3.5}$ undergoes decomposition with the final products being $Sc_4Ti_3O_{12}$ and $TiO_2$. Simultaneous Rietveld refinements against powder X-ray and neutron diffraction data showed that $Sc_4Ti_3O_{12}$ also exists in the defect fluorite structure in space group $Fm\bar{3}m$ (225) with $a$ = 4.90077(4) Å. $Sc_4Ti_3O_{12}$ undergoes partial reduction in CO/Ar atmosphere to form $Sc_4Ti_3O_{11.69(2)}$.

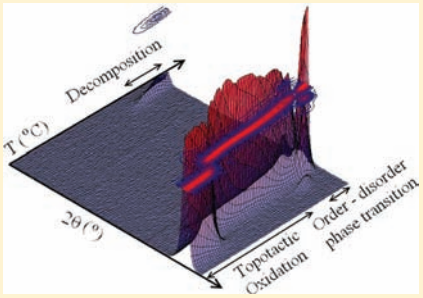


## 1. INTRODUCTION

Investigations of formation pathways of inorganic solids play a vital role in deducing structure−property relationships. In contrast to molecular sciences, reaction mechanisms are not well understood for extended solids. The recent advent of laboratory in-situ diffraction techniques allows investigation of solid-state reactions in real time.

$AVO_3$ phases with trivalent A cations (A = Ln, Sc, In, Y) are known to form either perovskites or bixbyites.[1−7] The ideal cubic perovskite structure described in space group $Pm\bar{3}m$ (Figure 1a) has a 12-fold-coordinated large A cation and 6-fold-coordinated smaller B cation. The $B−O_6$ octahedra form a corner-sharing infinite 3-dimensional network. Perovskite phases can undergo a number of distortions and cooperative tilts in order to accommodate differently sized A cations effectively. In contrast, the cubic bixbyite structure (Figure 1) is comprised of edge- and corner-sharing $(A/B)−O_6$ octahedra with statistical A and B cation disorder. Notably, the bixbyite structure accommodates the cations on 2 distinct sites (*8b* and *24d*). The *8b* site forms a regular octahedron, whereas the *24d* site is at the center of a distorted octahedron. Perovskite structures can be predicted with the Goldschmidt tolerance factor, $G_t = (A−O)/\sqrt{2}(B−O)$, where A−O and B−O correspond to the respective metal−oxygen bond distances. Perovskite phases are expected for $G_t$ values between 0.8 and 1.1.[8] For smaller A cations (e.g., $Sc^{3+}$ and $In^{3+}$) with tolerance factors less than 0.8 the $AVO_3$ compounds may crystallize in the cation-disordered bixbyite structure (Figure 1b).

We are interested in understanding solid-state reaction pathways with the potential benefit of controlling structures during synthesis. Understanding reaction sequences and solid-state reactivity will eventually provide insights into reaction mechanisms. Topotactic reactions involve modifications of structures while retaining substantial atomic connectivity of the precursor structures. Consequently, topotactic reactions do not require full reconstruction of the product crystal lattice. A recent review by Ranmohotti et al. discussed topochemical manipulations of perovskites in detail.[9]

Investigation of bixbyite phases and the structurally related fluorite structures with varying concentrations of oxide defects is motivated by their potential applications as solid-state oxide ion conductors.[22] Controlling the oxide defect concentrations and defect structures as well as evaluation of defect structure

**Received:** May 16, 2011
**Published:** January 24, 2012

   dx.doi.org/10.1021/ic201034x | *Inorg. Chem.* 2012, 51, 1269−1277

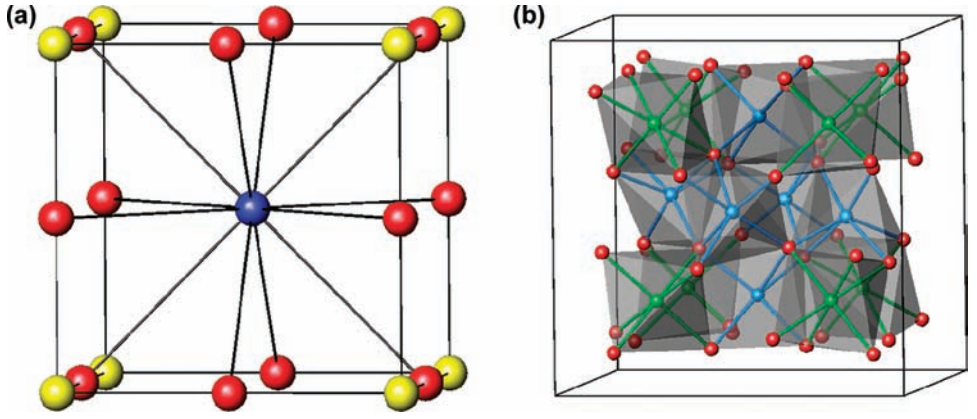


**Figure 1.** (a) Ideal cubic $ABO_3$ perovskite structure with 12-fold-coordinated A cation (blue sphere) and 6-fold-coordinated B cation (yellow spheres). (b) $ABO_3$ cubic bixbyite structure with A and B cation disorder arranged in $(A/B)-O_6$ regular (green) and distorted (blue) octahedral environment. Oxygen atoms are represented as red spheres in both structures.

stabilities is a crucial ingredient for the design of reliable high-performance oxide ion conductors for use in solid oxide fuel cells.

In 2004, Alonso et al. reported that the bixbyite $ScVO_3$ undergoes topotactic oxidation to form the defect fluorite $ScVO_{3.5}$ under relatively mild conditions.[4] Shafi et al.[10] showed that further oxidation of $ScVO_{3.5+x}$ results in the metastable intermediate $ScVO_{4-x}$ defect zircon structure prior to the topotactic oxidation to the fully oxidized $ScVO_4$ zircon phase. In addition, our work on the oxidation of $InVO_3$ bixbyite showed a similar metastable intermediate defect fluorite $InVO_{3.5+x}$ ($0.00 \leq x \leq 0.22$).[11] The structural relationship between bixbyite and defect fluorite phases has been discussed in detail.[11,12] Thus far, bixbyite oxidation pathway analysis has only been reported for vanadium-based compounds.

We are investigating the oxidation of $ScTiO_3$ bixbyite[13] in search of the previously unknown $ScTiO_{3.5}$ defect fluorite structure. The titanates provide a unique opportunity to stabilize this phase at high temperature because of the absence of higher oxidation states than 4+ for titanium. The $ScTiO_3$ oxidation pathway will enable us to generalize the oxidative pathway of bixbyite phases. In addition, a large concentration of oxide defects can be maintained at high temperatures in air for systematic investigation of oxide defects for oxide ion conductor applications. Our investigation of the $ScTiO_3$ oxidation pathway via in-situ X-ray diffraction covers the entire phase diagram. To the best of our knowledge, very few phases are known in the Sc−Ti−O phase diagram, namely, $ScTiO_3$,[13] $Sc_2TiO_5$,[14] $(Sc_xTi_{1-x})_2O_3$,[15] $Sc_4Ti_3O_{12}$,[16,17] $Sc_9Ti_{10}O_{31.2}$,[18] and $Sc_2Ti_2O_7$.[19−21] We are reporting for the first time the novel oxygen-deficient phases of $ScTiO_{3.5}$ and $Sc_4Ti_3O_{12-x}$. As the maximum oxidation state for Ti is 4+, the oxygen stoichiometry in $ScTiO_{3.5}$ is restricted unlike in other $AVO_{3.5+x}$ (A = Sc, In) defect fluorite structures.

## 2. EXPERIMENTAL SECTION

**2.1. Synthesis.** Polycrystalline $ScTiO_3$ was prepared by conventional solid-state synthesis. Stoichiometric amounts of $Sc_2O_3$ (Alfa Aesar, 99.99%), $TiO_2$ (Alfa Aesar, 99.995%), and Ti metal (Alfa Aesar, 99.99%), according to eq 1, were ground in an agate mortar with acetone and pelletized. The pellet was heated for 4−5 h in a diffusion pump vacuum ($p < 10^{-4}$ mbar) at 1500 °C with one intermediate grinding using a Huettinger TIG 5/300 induction furnace equipped with a copper coil. Bulk $ScTiO_{3.5}$ (~500 mg) was synthesized according to eq 2 by heating $ScTiO_3$ at 800 °C for 5 h in air.

$$2Sc_2O_3 + 3TiO_2 + Ti \rightarrow 4ScTiO_3 \quad (1)$$

$$ScTiO_3 + 0.25O_2 \rightarrow ScTiO_{3.5} \quad (2)$$

Polycrystalline $Sc_4Ti_3O_{12}$ was prepared by heating stoichiometric amounts of $Sc_2O_3$ (Alfa Aesar, 99.99%) and $TiO_2$ (Alfa Aesar, 99.995%) at 1500 °C in air for 12 h according to eq 3. $Sc_4Ti_3O_{12}$ was reduced in CO/Ar (1:3 ratio) flow in a tube furnace at 1500 °C, resulting in formation of the oxide defect phase $Sc_4Ti_3O_{12-x}$ according to eq 4.

$$2Sc_2O_3 + 3TiO_2 \rightarrow Sc_4Ti_3O_{12} \quad (3)$$

$$Sc_4Ti_3O_{12} + xCO \rightarrow Sc_4Ti_3O_{12-x} + xCO_2 \quad (4)$$

**2.2. Room-Temperature Powder X-ray Diffraction.** All products were identified using a PANalytical X'Pert Pro powder X-ray diffractometer with Cu $K\alpha_{1,2}$ ($\lambda$ = 1.540598 Å, 1.544426 Å) radiation equipped with a diffracted beam Ni filter and an X'Celerator detector operated in Bragg−Brentano geometry. The room-temperature diffractograms were collected from 10° to 120° in $2\theta$ with a step width of 0.0083°. Phase identification (using PDF2003), preliminary indexing, and space group determination were carried out with X'Pert Highscore Plus (version 2.1). The powder X-ray diffraction data sets were analyzed in detail by the Rietveld method using FullProf 2008.[23]

**2.3. High-Temperature Powder X-ray Diffraction.** High-temperature powder X-ray diffraction experiments were carried out on a PANalytical X'Pert Pro diffractometer equipped with a diffracted beam Ni filter, an X'celerator detector, and an Anton Paar HTK2000 high-temperature camera. Polycrystalline $ScTiO_3$ was heated on a resistive platinum strip heater from 25 to 1300 °C in air. Using Cu $K\alpha_{1,2}$ ($\lambda$ = 1.540598 Å, 1.544426 Å) radiation diffraction patterns were collected in 20 °C increments covering the angular range $15° \leq 2\theta \leq 120°$ with a 0.0167° step size. Using the same conditions thermal expansion experiments were conducted for $ScTiO_{3.5}$ and $Sc_4Ti_3O_{12}$ from 25 to 1300 °C at 50 °C increments in air.

**2.4. Multiphase High-Temperature in-Situ Rietveld Refinements.** The Rietveld refinements during heating of $ScTiO_3$ in air were conducted with typically 28−37 parameters for 1, 2, and 3 phases depending on the temperature range as indicated below.

(i) 25 °C ≤ $T$ ≤ 220 °C: 1 phase, $ScTiO_3$ cubic bixbyite phase
(ii) 240 °C ≤ $T$ ≤ 300 °C: 2 phases, $ScTiO_3$ cubic bixbyite and $ScTiO_{3.5}$ defect fluorite phases
(iii) 320 °C ≤ $T$ ≤ 840 °C: 1 phase, $ScTiO_{3.5}$ defect fluorite phase
(iv) 860 °C ≤ $T$ ≤ 920 °C: 2 phases, Sc-rich and Ti-rich cubic fluorite defect phases


dx.doi.org/10.1021/ic201034x | Inorg. Chem. 2012, 51, 1269−1277

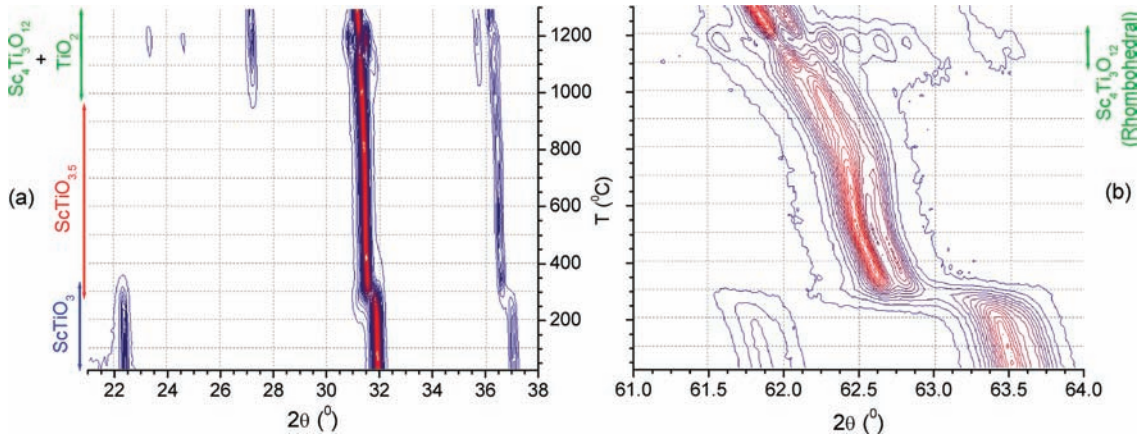


**Figure 2.** In-situ X-ray diffraction contour plot ((a) $21° \leq 2\theta \leq 38°$ and (b) $61° \leq 2\theta \leq 64°$) of $ScTiO_3$ oxidation in air from 25 to 1300 °C at 20 °C increments. Diffraction peak intensities are shown as constant increment contours from blue (lowest intensity) to red (highest intensity).

(v) 940 °C $\leq T \leq$ 1060 °C: 3 phases, Sc-rich and Ti-rich cubic defect fluorite phases and $TiO_2$ rutile
(vi) 1080 °C $\leq T \leq$ 1240 °C: 3 phases, cubic and rhombohedral $Sc_4Ti_3O_{12}$ phases and $TiO_2$ rutile
(vii) 1260 °C $\leq T \leq$ 1300 °C: 2 phases, cubic $Sc_4Ti_3O_{12}$ defect fluorite phase and $TiO_2$ rutile.

For all data sets the unit cell parameters, scale factors, peak shape parameters, temperature factors, background parameters, and sample height were refined. No atomic positions were refined for the high-temperature structures. The $\chi^2$ values for all but two refinements were consistently between 2.0 and 2.9. More details are provided in the Supporting Information.

**2.5. Room-Temperature Powder Neutron Diffraction.** Room-temperature powder neutron diffraction data for $ScTiO_3$ were collected on the medium-resolution 800-wire diffractometer C2 operated by the National Research Council Canada in Chalk River. The diffraction patterns were measured with neutron wavelengths $\lambda$ = 2.37248(15) Å ($4° \leq 2\theta \leq 84°$) and 1.33076(10) Å ($35° \leq 2\theta \leq 115°$) with 0.1° step sizes. Room-temperature powder neutron diffraction data for $ScTiO_{3.5}$ and $Sc_4Ti_3O_{12}$ were collected on the high flux diffractometer D20[24] at the Institut Laue-Langevin (ILL) in Grenoble with $\lambda$ = 1.8674(3) Å (germanium (115) reflection with a monochromator takeoff angle of 118°). Simultaneous powder neutron and powder X-ray refinements were carried out with FullProf 2008.[23]

**2.6. Thermogravimetric Analysis/Differential Thermal Analysis (TGA/DTA).** Simultaneous thermogravimetric and differential thermal analysis (TGA/DTA) experiments were carried out with a Linseis L81 thermobalance. $ScTiO_3$ (approximately 43 mg) was heated from 25 to 1450 °C and then cooled to room temperature in static air at a rate of 20 °C/min. Experiments were conducted in alumina crucibles with an empty crucible as the reference. The buoyancy correction was carried out with an empty crucible in the sample position. $Sc_4Ti_3O_{12-x}$ (approximately 49 mg) was heated from 25 to 1400 °C at 20 °C/min in oxygen flow and then cooled to room temperature at 60 °C/min. Experiments were corrected for buoyancy and conducted in alumina crucibles with $Al_2O_3$ as the reference. All products were identified by powder X-ray diffraction.

## 3. RESULTS AND DISCUSSION

**3.1. $ScTiO_3$ Bixbyite Oxidation Pathway, $ScTiO_{3.5}$/$Sc_4Ti_3O_{12}$ Formation, and High-Temperature Order–Disorder Transitions.** $ScTiO_3$ crystallizes in the reported[13] cubic bixbyite structure in space group $Ia\bar{3}$ (206) with scandium and titanium disorder on the *8b* and *24d* sites. The unit cell parameter $a$ = 9.7099(4) Å is in agreement with the previously reported value of $a$ = 9.709(3) Å by Reid et al.[13] Below we report the detailed structure of $ScTiO_3$ as determined by powder X-ray and neutron diffraction. Our previous work on topotactic oxidations of bixbyite phases[10,11] prompted our in-situ powder diffraction study of the oxidation pathway of $ScTiO_3$. Figure 2 ((a), $21° \leq 2\theta \leq 38°$ and (b), $61° \leq 2\theta \leq 64°$) is the contour plot of the temperature-dependent powder X-ray diffractograms during $ScTiO_3$ oxidation in air.

The contour plot shows $ScTiO_3$ persisting up to approximately 300 °C; the onset of new peaks belonging to an intermediate phase at around 240 °C indicate oxidation of $ScTiO_3$. This intermediate phase is stable up to 840 °C. The diffractograms of this novel phase resemble that of $ScVO_{3.5}$[4] and $InVO_{3.5}$[11] and can be indexed on a cubic unit cell with space group $Fm\bar{3}m$. In analogy to $ScVO_{3.5}$ and $InVO_{3.5}$ the novel intermediate is an oxygen-deficient fluorite phase with composition $ScTiO_{3.5}$. The low oxidation temperature (250–300 °C) suggests that oxidation proceeds topotactically. This is also in agreement with the close structural relation between the bixbyite and the fluorite structure.[4,11,12]

Above 920 °C, $ScTiO_{3.5}$ undergoes decomposition into $TiO_2$ (rutile) and another scandium titanate phase consistent with space group $Fm\bar{3}m$. The diffraction pattern of the defect fluorite phase observed at $T \geq$ 940 °C matches $Sc_4Ti_3O_{12}$ (ICDD powder X-ray diffraction reference code 00-031-1227). At 1080 °C $\leq T \leq$ 1240 °C the appearance of new peaks can be observed in Figure 2a and very prominently in Figure 2b. These additional peaks can be indexed on a rhombohedral unit cell in $R\bar{3}$ space group and are consistent with the anion-ordered $Sc_4Ti_3O_{12}$ structure.[16] Since the anion-ordered (rhombohedral) and cation-disordered (cubic) $Sc_4Ti_3O_{12}$ phases coexist between $T$ = 1080 and 1240 °C, the disorder–order phase transition is first order.

*3.1.1. Unit Cell Dimension Evolution During Oxidation and Annealing.* Figure 3(top) shows the cubic unit cell volume evolution of $Sc_yTi_zO_{3+x}$ as a function of temperature during in-situ oxidation of $ScTiO_3$. The initial linear volume increase is due to thermal expansion of $ScTiO_3$ (blue solid circles) followed by an up-turn, indicating oxygen uptake until 300 °C has been reached. From 250 °C the unit cell volume of the oxygen defect fluorite structure $ScTiO_{3.5-x}$ (red solid circles) increases until all $Ti^{3+}$ has been oxidized to $Ti^{4+}$. The concave rather than linear volume evolution between 400 and 700 °C is possibly due to oxide defect randomization in the $ScTiO_{3.5}$ structure. The thermal expansion of fully characterized (see below) $ScTiO_{3.5}$ and $Sc_4Ti_3O_{12}$ were determined in two


dx.doi.org/10.1021/ic201034x | Inorg. Chem. 2012, 51, 1269–1277

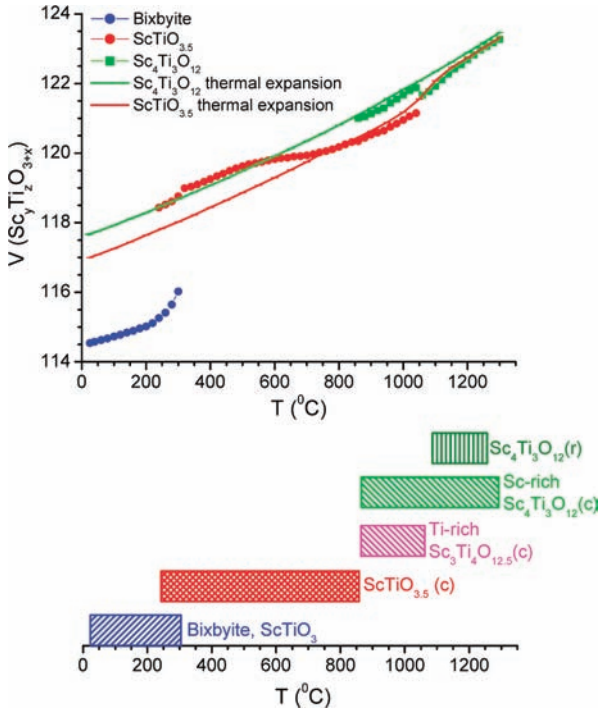


**Figure 3.** (Top) Formula unit volume evolution for cubic $Sc_yTi_zO_{3+x}$ structures as a function of temperature during in-situ powder X-ray diffraction in air. Bixbyite evolution is shown in blue solid circles, $ScTiO_{3.5}$ defect fluorite structure evolution in red solid circles, and $Sc_4Ti_3O_{12}$ defect fluorite structure evolution in green solid rectangles. Unit cell volume evolution due to thermal expansion for $ScTiO_{3.5}$ and $Sc_4Ti_3O_{12}$ is shown by the red solid line and green solid line, respectively. (Bottom) Temperature stability range for various phases observed during oxidation of $ScTiO_3$ bixbyite. Ti-rich regime is represented as $Sc_3Ti_4O_{12.5}$ and Sc-rich regime as $Sc_4Ti_3O_{12}$ for the temperature range $T$ = 860−1060 °C for convenience. Letters in the parentheses stand for c = cubic and r = rhombohedral.

separate in-situ diffraction experiments in air; unit cell evolutions are plotted as solid lines in Figure 3(top). The nearly linear increase between 700 and 850 °C (red solid circles) is attributed to the thermal expansion of the vacancy randomized $ScTiO_{3.5}$ structure since it is consistent with thermal expansion data for annealed $ScTiO_{3.5}$ (red solid line), which was measured independently. It is noteworthy that the unit cell volume (red solid circle) of the topotactic product during oxidation of the bixbyite phase is in perfect agreement with that of $ScTiO_{3.5}$ (red solid line) during thermal expansion at 800 °C. From 860 to 1060 °C the existing phases have closely related unit cell dimensions; both are cubic phases in $Fm\bar{3}m$ space group. Figure 3(top) shows that between this temperature range the unit cell volume of the phases deviate from the thermal expansion data for $ScTiO_{3.5}$ (red solid line); this suggests that $ScTiO_{3.5}$ undergoes phase separation into Sc-rich and Ti-rich defect fluorite phases. Interestingly, the phase with the larger unit cell volume (solid green rectangles) agrees with the thermal expansion of $Sc_4Ti_3O_{12}$ (green solid line) indicative of a Sc-rich phase, and the phase with smaller unit cell volume (red circles) falls below the thermal expansion of $ScTiO_{3.5}$ (red solid line) indicative of a Ti-rich phase. The Ti-rich phase must be part of the solid solution $Sc_{3+x}Ti_{4-x}O_{12+\delta}$ ($0 < x < 0.5$) but for convenience will be written as $Sc_3Ti_4O_{12.5}$ for the remainder of the text. Loss of $TiO_2$ begins at $T \approx$ 940 °C; this would most probably be occurring from the Ti-rich phase (assigned as $Sc_3Ti_4O_{12.5}$) in a continuous fashion until it reaches the composition $Sc_4Ti_3O_{12}$. Loss of $TiO_2$ increases the effective cationic radius on the *4a* site due to the $Sc^{3+}$ to $Ti^{4+}$ ratio increase which is observable by the increase in slope of the unit cell volume (red solid circles to green solid rectangles). Thermal expansion of $Sc_4Ti_3O_{12}$ (green solid line) is in very good agreement with this increased slope (green solid rectangles), and hence, the composition at high temperature during the in-situ study can be assigned as $Sc_4Ti_3O_{12}$. The bottom panel in Figure 3 represents the temperature ranges for various observed phases during oxidation of $ScTiO_3$. The Ti-rich regime is represented as $Sc_3Ti_4O_{12.5}$ and the Sc-rich regime as $Sc_4Ti_3O_{12}$ for the temperature range $T$ = 860−1060 °C for convenience in Figure 3(bottom). A small (peak height <6%) X-ray diffraction peak at $2\theta \approx 31.7°$ was observed between 1000 and 1160 °C and excluded from the refinements. This peak matches the hexagonal $Sc_9Ti_{10}O_{31.2}$ phase (ICDD powder X-ray diffraction reference code 00-031-1228).

*3.1.2. Phase Fraction Analysis during in-Situ Oxidation and Annealing.* The phase fractions during the entire process were also determined through Rietveld refinements of high-temperature in-situ X-ray diffraction data. The results are summarized in Figures 4 and 5. Figure 4 shows the phase

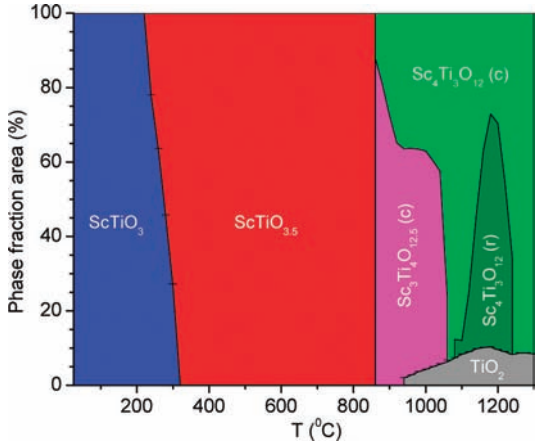


**Figure 4.** Phase fraction (%) of $Sc_zTi_yO_{3+x}$ from 25 to 1300 °C (blue = $ScTiO_3$, red = $ScTiO_{3.5}$, light green = Sc-rich cubic $Sc_4Ti_3O_{12}$, magenta = Ti-rich cubic $Sc_3Ti_4O_{12.5}$, dark green = rhombohedral $Sc_4Ti_3O_{12}$, gray = $TiO_2$).

fraction (%) of $Sc_yTi_zO_{3+x}$ from 25 to 1300 °C. Formation of the topotactic oxidation product begins at 240 °C, and all of the $ScTiO_3$ bixbyite (blue region) oxidized at 320 °C to the defect fluorite $ScTiO_{3.5}$ (red region). At 860 °C the $ScTiO_{3.5}$ phase segregates into Sc-rich (light green region, represented as $Sc_4Ti_3O_{12}$ in Figure 4) and Ti-rich (magenta region, represented as $Sc_3Ti_4O_{12.5}$ in Figure 4) phases. With the increase in temperature the phase fraction of the Sc-rich phase increases and that of the Ti-rich phase decreases; this is consistent with the onset of $TiO_2$ rutile phase formation, which is observed at 920 °C. At 1080 °C the Ti-rich phase disappears as it completely converts to $Sc_4Ti_3O_{12}$ expelling $TiO_2$. At 1080 °C a fraction of the $Sc_4Ti_3O_{12}$ phase undergoes a phase transition from the cation-disordered cubic (light green region) to an oxide defect-ordered rhombohedral structure (dark green region). The rhombohedral phase (dark green region) disappears at 1260 °C and forms the entropically favored


dx.doi.org/10.1021/ic201034x | *Inorg. Chem.* 2012, 51, 1269−1277

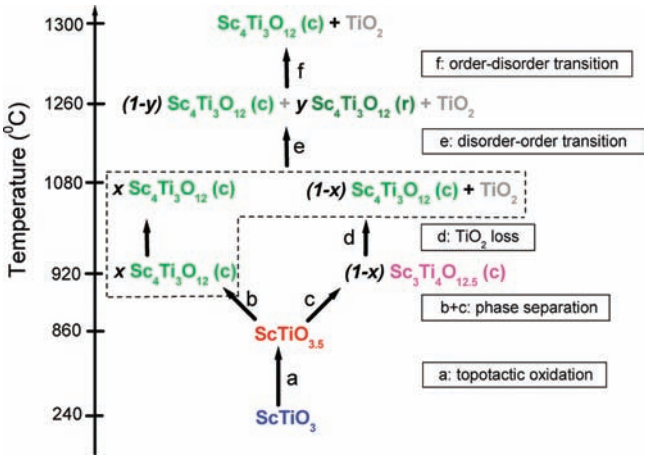


**Figure 5.** Flowchart of the proposed mass unbalanced reaction pathway for $ScTiO_3$ bixbyite oxidation. For convenience, Sc-rich and Ti-rich phases are represented as $Sc_4Ti_3O_{12}$ and $Sc_3Ti_4O_{12.5}$, respectively. Letters in the parentheses stand for c = cubic and r = rhombohedral.

cation-disordered cubic structure (light green region) at high temperature.

*3.1.3. Summary of in-Situ Oxidation and Annealing.* The entire reaction process is summarized below and presented as a flowchart in Figure 5.

At 240 °C, shown as step a in Figure 5, $ScTiO_3$ oxidizes topotactically to $ScTiO_{3.5}$

$$ScTiO_3 + 0.25O_2 \rightarrow ScTiO_{3.5} \quad (240\ ^\circ C \leq T \leq 840\ ^\circ C) \qquad (a)$$

The second step b + c in Figure 5 represents phase separation of $ScTiO_{3.5}$ into $Sc_4Ti_3O_{12}$ and $Sc_3Ti_4O_{12.5}$

$$ScTiO_{3.5} \rightarrow xSc_4Ti_3O_{12} + (1 - x)Sc_3Ti_4O_{12.5} \quad (860\ ^\circ C \leq T \leq 920\ ^\circ C) \qquad (b + c)$$

Step d indicates loss of $TiO_2$ from $Sc_3Ti_4O_{12.5}$ with formation of $Sc_4Ti_3O_{12}$

$$(1 - x)Sc_3Ti_4O_{12.5} \rightarrow 0.75(1 - x)Sc_4Ti_3O_{12} + 7/4(1 - x)TiO_2 \quad (940\ ^\circ C \leq T \leq 1060\ ^\circ C) \qquad (d)$$

Step e corresponds to the cubic (c) to rhombohdral (r) phase transition of a fraction of $Sc_4Ti_3O_{12}$

$$Sc_4Ti_3O_{12} + TiO_2 \rightarrow (1 - y)Sc_4Ti_3O_{12}(c) + ySc_4Ti_3O_{12}(r) + TiO_2 \quad (1080\ ^\circ C \leq T \leq 1240\ ^\circ C) \qquad (e)$$

In the final step f the rhombohedral $Sc_4Ti_3O_{12}$ phase fraction converts back to the entropically favored cubic structure

$$(1 - y)Sc_4Ti_3O_{12}(c) + ySc_4Ti_3O_{12}(r) + TiO_2 \rightarrow Sc_4Ti_3O_{12}(c) + TiO_2 \quad (1260\ ^\circ C \leq T \leq 1300\ ^\circ C) \qquad (f)$$

The complex reaction pathway involves topotactic oxidation, phase segregation, and order−disorder phase transitions. Notably, our findings based on unit cell volume evolution (which is traced back to diffraction peak positions) and phase fraction analyses (which can be traced back to diffraction peak intensities) are in excellent agreement. The fact that all phases with the exception of the high-temperature rhombohedral structure are cubic is advantageous for this detailed analysis.

The TGA/DTA data in Figure 6 complement the in-situ powder X-ray diffraction experiments. The simultaneous

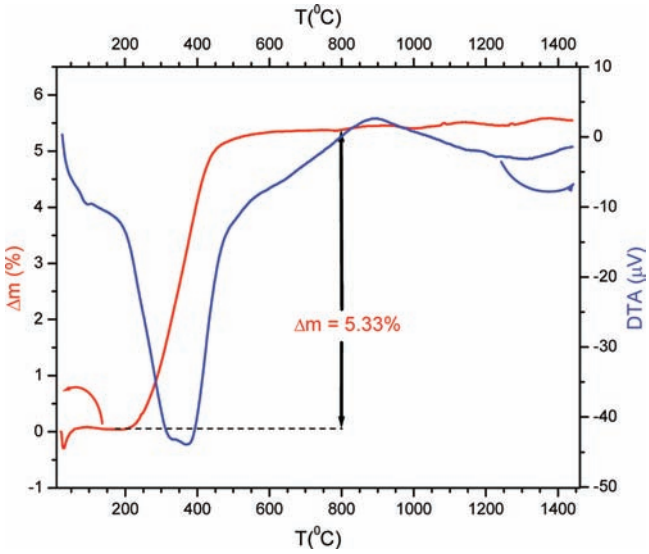


**Figure 6.** TGA/DTA oxidation of $ScTiO_3$ in air from 25 to 1450 °C at a heating rate of 20 °C/min. Red and blue lines indicate TGA and DTA curves, respectively, the solid arrow indicates the mass gain observed from room temperature to 800 °C, and the dashed line is only a guide to the eye.

presence of an exothermic peak at 375 °C in the DTA curve and the mass gain in the TGA data (inflection point at 375 °C) correspond to oxidation of $ScTiO_3$ to $ScTiO_{3.5}$. The observed mass gain of 5.33% (shown as a solid arrow in Figure 6) indicates that the product at 800 °C is $ScTiO_{3.47(2)}$. The plateau of the TGA curve beyond 500 °C suggests complete oxidation with no further mass changes upon extended heating. The poorly resolved broad DTA feature at $T \approx 900$ °C is likely due to formation of $TiO_2$ rutile, phase segregation into the Sc-rich and Ti-rich phases, as well as the onset of the ordered rhombohedral $Sc_4Ti_3O_{12}$ phase. The final product only consisted of cubic $Sc_4Ti_3O_{12}$ and $TiO_2$ rutile at room temperature.

From these experiments the appropriate conditions for the bulk preparation of $ScTiO_{3.5}$ were determined. $ScTiO_{3.5}\square_{0.5}$ (where □ denotes oxide defects) crystallizes in the fluorite structure with 0.5 oxide defects (12.5% of the fluorite oxide lattice). Oxidizing $ScTiO_3$ ex situ for 5 h at 800 °C in either air or oxygen is sufficient to form a fully equilibrated $ScTiO_{3.5}$ oxide defect fluorite sample. The in-situ studies showed a lack of randomization of the oxide defects in $ScTiO_{3.5}$ at lower temperatures, possibly due to insufficient annealing time during the relatively fast in-situ experiment.

The in-situ powder X-ray diffraction experiments of $ScTiO_{3.5}$ and $ScVO_{3.5+x}$[11] in air contrast their respective stability ranges. $ScVO_{3.5}$ oxidizes to $ScVO_4$ at approximately 425 °C, whereas


dx.doi.org/10.1021/ic201034x | Inorg. Chem. 2012, 51, 1269−1277

$ScTiO_{3.5}$ is stable up to 925 °C subsequently forming $Sc_4Ti_3O_{12}$ and $TiO_2$.

**3.2. Structural Analysis of $ScTiO_3$, $ScTiO_{3.5}$, and $Sc_4Ti_3O_{12}$ Phases Involved in the Topotactic Oxidation.** *3.2.1. $ScTiO_3$ Structure.* We report the first powder neutron diffraction study on the $ScTiO_3$ bixbyite phase. The neutron data are particularly important in order to identify Sc/Ti preference on the two cation sites, to accurately determine the oxygen sublattice, and consequently to obtain reliable coordination polyhedra. The 4-histogram Rietveld refinement was carried out for one X-ray and three neutron diffractograms using FullProf 2008.[23] A total of 38 parameters including neutron wavelength, zero point, unit cell parameter, scale factors, peak shape parameters, temperature factors, atomic positions, and site occupancies were refined. It should be noted that the site occupancies were constrained to be fully occupied; thus, the Sc/Ti ratios were refined independently for both sites. The background was fitted for the initial least-squares cycles using a cubic spline and fixed for the following cycles. The Rietveld plots are shown in Figure 7, and the structural details

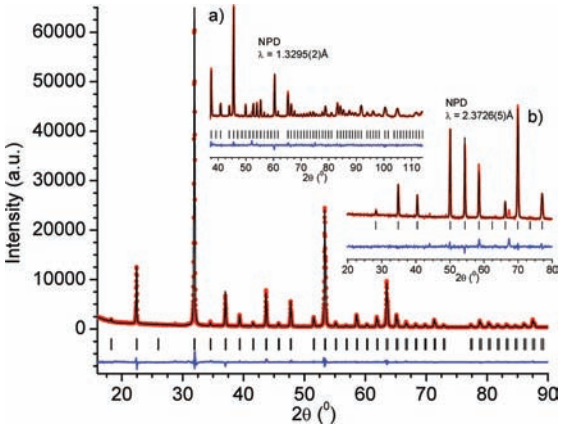


**Figure 7.** Rietveld plots for $ScTiO_3$ room-temperature refinement. Powder X-ray diffraction data Cu $K_{\alpha 1,2}$ radiation and powder neutron diffractograms $\lambda$ = (a) 1.3295(2) and (b) 2.3726(5) Å. Red circles = experimental data, black line = best fit, blue line = difference, black tick marks = Bragg positions.

are provided in Table 1. The refined occupancies indicate a site preference of $Ti^{3+}$ for the *8b* site and a small $Sc^{3+}$ preference for the *24d* site. The refined composition $Sc_{0.969(6)}Ti_{1.025(6)}O_3$ is in excellent agreement with the nominal composition. The bond valences (determined with VaList[25]) confirm these cation preferences. There is no indication of cation ordering in $ScTiO_3$.

*3.2.2. $ScTiO_{3.5}$ Structure.* Room-temperature X-ray and neutron powder diffraction data were collected on a bulk sample of $ScTiO_{3.5}$, and the Rietveld analysis was carried out with FullProf 2008.[23] $ScTiO_{3.5}$ crystallizes in the defect fluorite structure in space group $Fm\bar{3}m$ (225) with $a$ = 4.89199(5) Å. For the 2 histogram refinements a total of 19 parameters including peak shape parameters, scale factors, neutron wavelength, unit cell parameter, temperature factors, cation occupancies, and zero points were refined. The backgrounds were fitted using a cubic spline during the initial cycles and fixed for subsequent cycles. The Rietveld plots for $ScTiO_{3.5}$ refined in space group $Fm\bar{3}m$ are shown in Figure 8, and structural details are provided in Table 2. The $Sc^{3+}/Ti^{4+}$ cations occupy the *4a* (0, 0, 0) site in a disordered fashion, and the

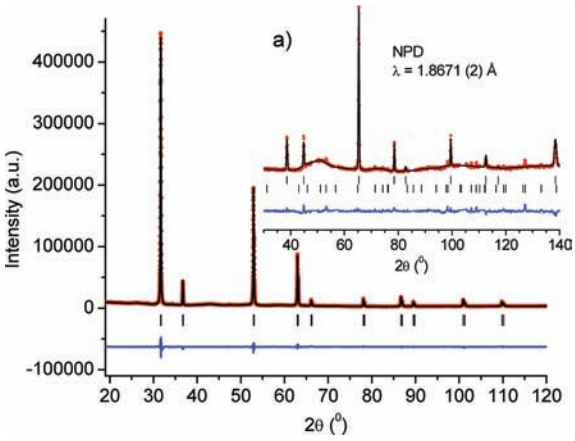


**Figure 8.** Rietveld plots of $ScTiO_{3.5}$ room-temperature refinement. Powder X-ray diffraction data Cu $K\alpha_{1,2}$ radiation and powder neutron diffractogram (insert) with $\lambda$ = 1.8671(2) Å. Red circles = experimental data, black line = best fit, blue line = difference, black tick marks = Bragg positions. In the neutron powder diffractogram (insert), top tick marks are $ScTiO_{3.5}$ Bragg position and bottom marks are that of $Al_2O_3$. Pt peaks originating from the sample container in the neutron data have been excluded from the refinement.

oxide anion is located on the *8c* (1/4, 1/4, 1/4) site with an occupancy of 0.875. The bond valences (determined with VaList[25]) indicate the presence of $Sc^{3+}$ (BV = 3.9) and $Ti^{4+}$ (BV = 3.5) on one site. The large oxygen temperature factor of 5.15 (3) $Å^2$ is due to the large defect concentration and the associated disorder on the oxide sublattice in that structure. The absence of superstructure peaks in the X-ray and neutron diffractograms rules out any potential ion/defect ordering. The powder neutron diffraction pattern showed a broad peak at $d \approx$ 2.14 Å which is not observed in the X-ray diffraction pattern. A similar feature was observed in $AVO_{3.5+x}$ neutron diffraction patterns, and it has been suggested that this is due to oxygen defect clusters.[10] Small impurity peaks from $Al_2O_3$ corundum which was used as a thermocouple sleeve for the high-temperature measurements was found in the room-temperature neutron powder diffractogram for $ScTiO_{3.5}$; the Bragg peak positions are shown in Figure 8 (insert) as bottom tick marks. In the fluorite structure cations form a cubic close-packed structure with anions in the tetrahedral interstitials. The average oxide defect fluorite structure can be derived from the parent fluorite structure as illustrated in Figure 9. In this defect fluorite structure one of the eight oxide ion positions is vacant. The randomly chosen oxide ion vacancy is shown as the yellow sphere in Figure 9. As expected during a topotactic oxidation of $ScTiO_3$ to $ScTiO_{3.5}$ no cation migration occurs. The oxygen uptake increases the average cation coordination from six to seven. Formation of defect fluorite $ABO_{3.5}$ is entirely dependent on the structure of the $ABO_3$ bixbyite starting material; our previous work has shown that perovskite phases do not form this metastable product during oxidation.[7,11] Ex-situ experiments showed that at elevated temperatures $T$ > 800 °C $ScTiO_{3.5}$ decomposes into $TiO_2$ rutile and cubic $Sc_4Ti_3O_{12}$. We suggest that the driving force behind the decomposition of $ScTiO_{3.5}$ is the thermodynamic stability of the rutile phase.

*3.2.3. $Sc_4Ti_3O_{12}$ Structure.* It is noteworthy that there are only two entries in the ICSD and PDF2003 corresponding to $Sc_4Ti_3O_{12}$, namely, an anion ordered rhombohedral structure and a cation-disordered cubic defect fluorite structure. Diffraction patterns obtained at $T \geq$ 900 °C during in-situ


dx.doi.org/10.1021/ic201034x | Inorg. Chem. 2012, 51, 1269–1277

**Table 1. Structural Parameters, Bond Angles, and Average Bond Distances for $ScTiO_3$ Bixbyite Phase (space group $Ia\bar{3}$ (No. 206)) As Obtained from Rietveld Refinements against Three Neutron and One X-ray Diffraction Pattern Measured at Room Temperature**

| | | |
|---|---|---|
| composition | | $ScTiO_3$ |
| unit cell content | | $Sc_{15.5(1)}Ti_{16.4(1)}O_{48}$ |
| $T$ (K) | | 295 |
| space group | | $Ia\bar{3}$(206) |
| unit cell | $a$ (Å) | 9.7099(4) |
| | $V$ (Å$^3$) | 915.47(7) |
| Sc/Ti (*8b*) (1/4, 1/4, 1/4) | $B_{iso}$ (Å$^2$) | 0.76(9) |
| | Occ. (Sc) | 0.281(5) |
| | Occ. (Ti) | 0.719(5) |
| Sc/Ti (*24d*) ($x$, 0, 1/4) | $x/a$ | 0.9665(1) |
| | $B_{iso}$ (Å$^2$) | 0.66(5) |
| | Occ. (Sc) | 0.554(3) |
| | Occ. (Ti) | 0.446(3) |
| O (*48e*) ($x$, $y$, $z$) | $x/a$ | 0.3905(3) |
| | $y/b$ | 0.1553(2) |
| | $z/c$ | 0.3812(3) |
| | $B_{iso}$ (Å$^2$) | 0.43(4) |
| | Occ. (O) | 1.000 (fixed) |
| $d$(Sc(1)/Ti(1))−O (Å) | | 6 × 2.081(2) |
| $d$(Sc(2)/Ti(2))−O (Å) | | 2 × 2.143(2) |
| | | 2 × 2.108(2) |
| | | 2 × 2.040(2) |
| average $d$(Sc(2)/Ti(2)−O | | 2.097(2) |
| bond valences | Sc(1) | 3.348, 43% (0.28) |
| BV, site occupancy based on BV (site occupancy from refinement) | Ti(1) | 2.742, 57% (0.72) |
| | Sc(2) | 3.226, 61% (0.55) |
| | Ti(2) | 2.642, 39% (0.45) |
| no. of params | | 38 |
| $Z$ | | 16 |
| $R$ values | XRD[a] (Rp, Rwp, $\chi^2$) | 4.39/5.99/3.94 |
| | NPD-1[a] (Rp, Rwp, $\chi^2$) | 2.07/2.80/4.78 |
| | NPD-2[a] (Rp, Rwp, $\chi^2$) | 2.18/2.95/4.64 |
| | NPD-3[a] (Rp, Rwp, $\chi^2$) | 2.24/2.97/2.62 |

[a]X-ray: $K_{\alpha1,2}$, $\lambda$ = 1.540598 Å, 1.544426 Å, 10° ≤ 2$\theta$ ≤ 90°, Δ2$\theta$ = 0.0167°, 4781 data points, weight in refinement = 0.25. NPD-1: $\lambda$ = 1.3295(2) Å, 4.4° ≤ 2$\theta$ ≤ 84°, Δ2$\theta$ = 0.1003°, 795 data points, weight in refinement = 0.25. NPD-2: $\lambda$ = 1.3295(2) Å, 35.4° ≤ 2$\theta$ ≤ 115°, Δ2$\theta$ = 0.1003°, 795 data points, weight in refinement = 0.25. NPD-3: $\lambda$ = 2.3726(5) Å, 4.4° ≤ 2$\theta$ ≤ 84°, Δ2$\theta$ = 0.1003°, 795 data points, weight in refinement = 0.25.

**Table 2. Structural Parameters, Bond Angles, and Average Bond Distances for $ScTiO_{3.5}$ Oxygen-Deficient Cubic Fluorite Phase (space group $Fm\bar{3}m$ (No. 225)) as Obtained from Rietveld Refinements against One Neutron and One X-ray Diffraction Pattern Measured at Room Temperature**

| | | |
|---|---|---|
| composition | | $ScTiO_{3.5}$ |
| unit cell content | | $Sc_{1.94(2)}Ti_{2.05(2)}O_{7.00}$ |
| $T$ (K) | | 295 |
| space group | | $Fm\bar{3}m$ (225) |
| unit cell | $a$ (Å) | 4.89199(5) |
| | $V$ (Å$^3$) | 117.073(2) |
| Sc/Ti (4a) (0, 0, 0) | $B_{iso}$ (Å$^2$) | 2.43(1) |
| | Occ. (Sc) | 0.487(5) |
| | Occ. (Ti) | 0.513(5) |
| O (8c) (1/4, 1/4, 1/4) | $B_{iso}$ (Å$^2$) | 5.15 (3) |
| | Occ. | 0.875 |
| $d$(Sc(1)/Ti(1))−O (Å) | | 8 × 2.118292(4) |
| no. of params | | 19 |
| $Z$ | | 2 |
| $R$ values | XRD[a] (Rp, Rwp, $\chi^2$) | 2.90/4.30/11.6 |
| | NPD-1[a] (Rp, Rwp, $\chi^2$) | 3.18/4.42/3.04 |

[a]X-ray: $K_{\alpha1,2}$, $\lambda$ = 1.540598 Å, 1.544426 Å, 10° ≤ 2$\theta$ ≤ 120°, Δ2$\theta$ = 0.0083°, 13 158 data points, weight in refinement = 0.3. NPD-1: $\lambda$ = 1.8671(2) Å, 0.1° ≤ 2$\theta$ ≤ 150.9°, Δ2$\theta$ = 0.1001°, 1508 data points, weight in refinement = 0.7.

oxidation of $ScTiO_3$ matched the cubic defect fluorite phase $Sc_4Ti_3O_{12}$. The structural characteristics of $Sc_4Ti_3O_{12}$ were established via combined Rietveld refinements against powder X-ray and neutron diffraction data measured on bulk samples using FullProf 2008.[23] A total of 20 parameters including peak shape parameters, scale factors, neutron wavelength, unit cell parameter, temperature factors, occupancies of cations, and zero points were refined. The Rietveld refinement plots are shown in Figure 10, and the structural details are provided in

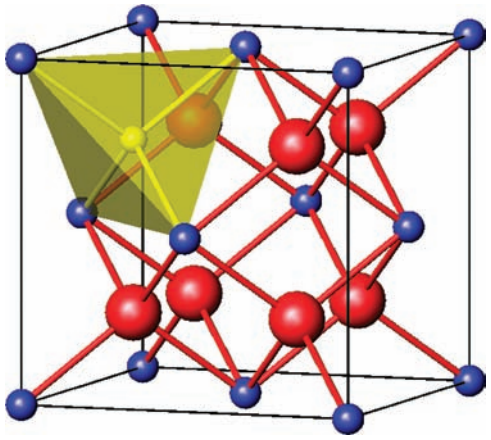

**Figure 9.** Fluorite structure with $Sc^{3+}/Ti^{4+}$ cations in blue and $O^{2-}$ anions in red. Randomly chosen oxygen defect is shown in the tetrahedral environment as a yellow sphere.

Table 3. $Sc_4Ti_3O_{12}$ exists in the defect fluorite structure in space group $Fm\bar{3}m$ with unit cell parameter $a$ = 4.90077(4) Å which is larger than that of $ScTiO_{3.5}$ due to more $Sc^{3+}$ ions in the former phase (Shannon radii $Sc^{3+}$(VI) = 0.745 Å, $Ti^{4+}$(VI) = 0.605 Å). The cations $Sc^{3+}/Ti^{4+}$ occupy the *4a* (0, 0, 0) site in a disordered fashion, and the oxide anion is located on the *8c* (1/4, 1/4, 1/4) site with an occupancy of 0.88. The bond valences (determined with VaList[25]) indicate the presence of $Sc^{3+}$ (BV = 3.8) and $Ti^{4+}$ (BV = 3.5) on one site. The particularly large oxygen temperature factor of 6.91(9) Å$^2$ is due to the large defect concentration in the structure. The composition calculated from the Rietveld refinement is $Sc_{2.16(1)}Ti_{1.84(1)}O_{7.03(4)}$ with $Z$ = 2.

**3.3. Partial Topotactic Reduction of $ScTiO_{3.5}$ and $Sc_4Ti_3O_{12}$.** Under strongly reducing conditions both defect fluorite phases $ScTiO_{3.5}$ ($H_2$ gas, 700 °C) and $Sc_4Ti_3O_{12}$ (CO gas, 1500 °C) showed partial reduction of $Ti^{4+}$ ions indicated by the


dx.doi.org/10.1021/ic201034x | Inorg. Chem. 2012, 51, 1269−1277

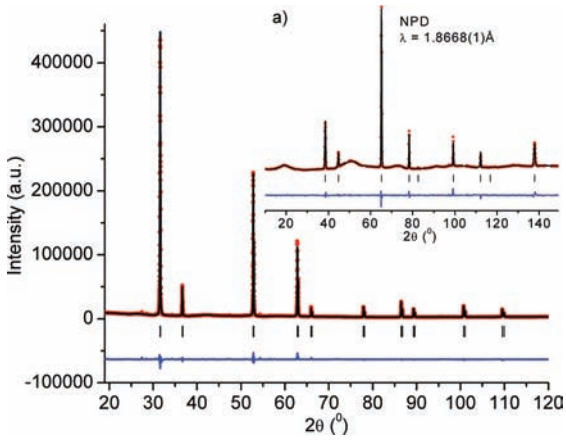


**Figure 10.** Rietveld plots for cubic $Sc_4Ti_3O_{12}$ at room temperature. Powder X-ray diffraction data, Cu K$\alpha_{1,2}$ radiation: (a) powder neutron diffractogram (D20) with $\lambda$ = 1.8668(1) Å. Red circles = experimental data, black line = best fit, blue line = difference, black tick marks = Bragg positions. Pt peaks originating from the sample container in the neutron data have been excluded from the refinement.

**Table 3. Structural Parameters, Bond Angles, and Average Bond Distances for $Sc_4Ti_3O_{12}$ Oxygen-Deficient Cubic Fluorite Phase (space group $Fm\bar{3}m$ (No. 225)) as Obtained from Rietveld Refinements against One Neutron and One X-ray Diffraction Pattern Measured at Room Temperature**

| | | |
|---|---|---|
| composition | | $Sc_4Ti_3O_{12}$ |
| unit cell content | | $Sc_{2.16(1)}Ti_{1.84(1)}O_{7.03(4)}$ |
| $T$ (K) | | 295 |
| space group | | $Fm\bar{3}m$ (225) |
| unit cell | $a$ (Å) | 4.90077(4) |
| | $V$ (Å$^3$) | 117.705(1) |
| Sc/Ti (4a) (0, 0, 0) | $B_{iso}$ (Å$^2$) | 3.28(2) |
| | Occ. (Sc) | 0.540(3) |
| | Occ. (Ti) | 0.460(3) |
| O (8c) (1/4, 1/4, 1/4) | $B_{iso}$ (Å$^2$) | 6.91(9) |
| | Occ. | 0.88(2) |
| $d$(Sc(1)/Ti(1))−O (Å) | | 8 × 2.12210(2) |
| no. of params | | 20 |
| $Z$ | | 2 |
| $R$ values | XRD[a] (Rp, Rwp, $\chi^2$) | 3.10/4.69/12.0 |
| | NPD-1[a] (Rp, Rwp, $\chi^2$) | 2.30/3.57/4.71 |

[a]X-ray: $K_{\alpha 1,2}$, $\lambda$ = 1.540598 Å, 1.544426 Å, 10° ≤ 2$\theta$ ≤ 120°, $\Delta 2\theta$ = 0.0083°, 13 158 data points, weight in refinement = 0.3. NPD-1: $\lambda$ = 1.8668(1) Å, 0.1° ≤ 2$\theta$ ≤ 150.9°, $\Delta 2\theta$ = 0.1001°, 1508 data points, weight in refinement = 0.7.

sample color change as well as the peak shift in the diffraction pattern. X-ray data for the (111) reflection of $Sc_4Ti_3O_{12}$ and $Sc_4Ti_3O_{12-x}$ and their respective sample colors are shown in Figure 11. These two materials are visibly distinguishable as $Sc_4Ti_3O_{12}$ is pale yellow while $Sc_4Ti_3O_{12-x}$ is black. Both phases produce the same diffraction patterns with an obvious peak position shift. $Sc_4Ti_3O_{12}$ peaks (red peaks) are shifted to lower angles compared to those of $Sc_4Ti_3O_{12-x}$ (green). Also, the XRD pattern of the mixture of these two phases (blue pattern shown as an insert in Figure 11) showed double peaks indicating that the phases have different unit cell dimensions. Figure 12 shows the TGA/DTA plot during oxidation of $Sc_4Ti_3O_{12-x}$ in oxygen with a single exotherm and a single-step

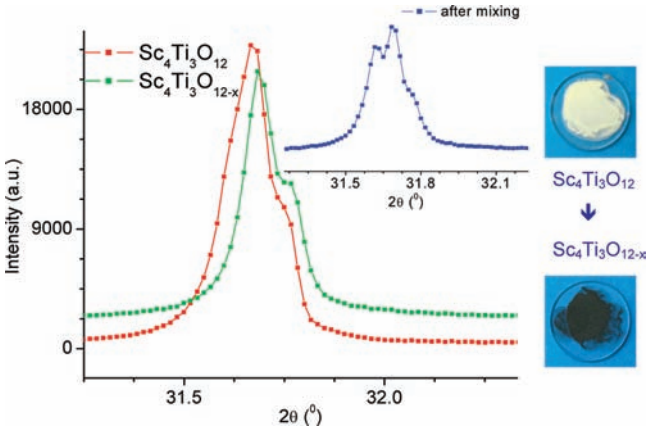


**Figure 11.** Powder X-ray diffraction patterns zoomed in to the (111) reflection of $Sc_4Ti_3O_{12}$ (red), $Sc_4Ti_3O_{12-x}$ (green), and the mixture (blue). Sample colors of $Sc_4Ti_3O_{12}$ and $Sc_4Ti_3O_{12-x}$ are compared on the righthand side.

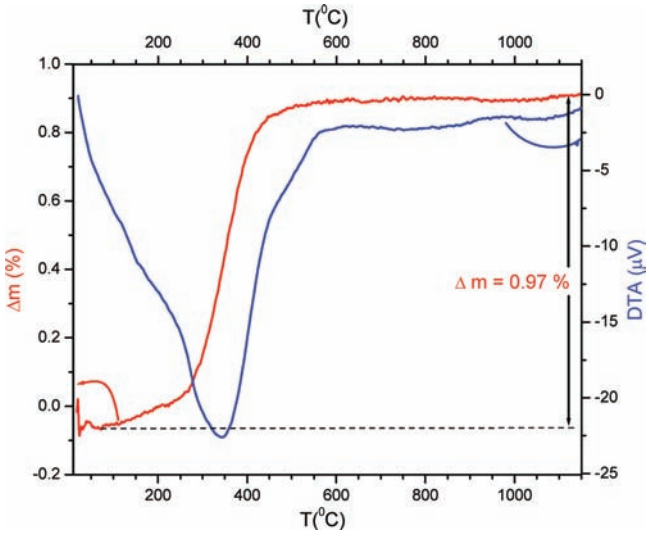


**Figure 12.** TGA/DTA oxidation of $Sc_4Ti_3O_{12-x}$ in air from 25 to 1400 °C at a heating rate of 20 °C/min. Red and blue lines indicate TGA and DTA curves, respectively, the solid arrow indicates the mass gain observed from room temperature to 1100 °C, and the dashed line is only a guide to the eye.

mass gain. The mass gain of 0.97% during oxidation indicates the composition of this unreported phase to be $Sc_4Ti_3O_{11.69(2)}$. The fully oxidized $Sc_4Ti_3O_{12}$ phase has a larger unit cell due to its larger oxygen content in comparison to the reduced $Sc_4Ti_3O_{12-x}$ phase. This trend is consistent with the redox behavior of the defect fluorite phases $AVO_{3.5+x}$ (A = Sc, In) where unit cell expansion was observed with increasing oxygen stoichiometry rather than cell contraction due to substitution of the larger $V^{4+}$ with the smaller $V^{5+}$ cation.[11]

## 4. SUMMARY AND CONCLUSIONS

We are reporting for the first time the synthesis, stability, and structure of the novel oxygen defect fluorite $ScTiO_{3.5}$. Oxidation of $ScTiO_3$ has been followed via in-situ X-ray diffraction and TGA/DTA experiments. The topotactic oxidation of the bixbyite phase $ScTiO_3$ resulted in formation of the related oxide defect structure $ScTiO_{3.5}$; this is an


dx.doi.org/10.1021/ic201034x | Inorg. Chem. 2012, 51, 1269−1277

extension of the previously published oxidation pathways of the vanadium-bearing bixbyite phases $ScVO_3$ and $InVO_3$ and therefore clearly illustrates a structure−reactivity relation. With this the present study emphasizes a generalized topotactic oxidation pathway for bixbyite phases. In addition to the initial topotactic oxidation step the present in-situ study has revealed complex phase equilibria between cubic $ScTiO_{3.5}$, $Sc_3Ti_4O_{12.5}$, and $Sc_4Ti_3O_{12}$ phases and an oxide ordered rhombohedral defect fluorite phase. $ScTiO_{3.5}$ crystallizes in the defect fluorite structure (space group $Fm\bar{3}m$) with $Sc^{3+}/Ti^{4+}$ disorder on the *4a* site and $O^{2-}$ anions occupying the *8c* site with 1/8 disordered defects. Neutron diffraction data suggest possible oxide defect clustering in $ScTiO_{3.5}$; the same has been reported for the vanadium analogues.[10] Only prolonged annealing of $ScTiO_{3.5}$ at 800 °C just below the initial formation temperature of $Sc_4Ti_3O_{12}$ results in a phase-pure homogeneous $ScTiO_{3.5}$ sample. Only at temperatures above 840 °C the cations become sufficiently mobile for phase separation into Sc-enriched as well as Sc-depleted cubic defect fluorite structures. Below that temperature the ion mobility and therefore the chemical reactivity appears to be limited to the oxide sublattice: the topotactic regime. The average coordination number of both cations in $ScTiO_{3.5}$ is seven. It appears that the observed phase transitions and phase separations are driven by enabling octahedral $Ti^{4+}$ coordination. This is the case for the rutile structure, which is found as a byproduct during $Sc_4Ti_3O_{12}$ formation and during oxide ordering where the resulting rhombohedral structure also has an octahedral site, which is assumed to be exclusively occupied by $Ti^{4+}$. Controlling the reactivity of sublattices and the corresponding ion mobilities in those oxide defect structures is particularly important for ion conductors and consequently for solid-state electrolytes in fuel cell applications. In-situ diffraction has matured into a powerful tool for tackling reaction pathway analysis for solid-state reactions and thus provides important information for the controlled synthesis of extended solids.

## ■ ASSOCIATED CONTENT

### Ⓢ Supporting Information

Details regarding the temperature-dependent Rietveld refinements against the powder X-ray diffraction data collected during in-situ $ScTiO_3$ oxidation. This material is available free of charge via the Internet at http://pubs.acs.org.

## ■ AUTHOR INFORMATION

### Corresponding Author

*Phone: (204) 474-6258. Fax: (204) 474-7608. E-mail: Mario_Bieringer@umanitoba.ca.

### Notes

[‖]Deceased.

## ■ ACKNOWLEDGMENTS

M.B. acknowledges NSERC and CFI for operating and infrastructure support. S.P.S. is thankful for graduate student support (UMGF) from the University of Manitoba. Dr. Holger Kleinke and Jackie Xu are acknowledged for synthesis of $ScTiO_3$. We thank the Institut Laue-Langevin (ILL) for providing neutron beam time and technical support. We acknowledge the National Research Council−Canadian Neutron Beam Centre (NRC−CNBC) for access to the neutron diffractometer C2 and technical support.

## ■ REFERENCES

(1) Mizokawa, T.; Khomskii, D. I.; Sawatzky, G. A. *Phys. Rev. B* **1999**, *60*, 7309.
(2) Ren, Y.; Palstra, T. T. M.; Khomskii, D. I.; Pellegrin, E.; Nugroho, A. A.; Menovsky, A. A.; Sawatzky, G. A. *Nature* **1998**, *396*, 441.
(3) Nguyen, H. C.; Goodenough, J. B. *Phys. Rev. B* **1995**, *52*, 324.
(4) Alonso, J. A.; Casais, M. T.; Martinez-Lope, M. J. *Dalton Trans.* **2004**, *9*, 1294.
(5) Miyasaka, S.; Okimoto, Y.; Iwama, M.; Tokura, Y. *Phys. Rev. B* **2003**, *68*, 100406.
(6) Lundgren, R. J.; Cranswick, L. M. D.; Bieringer, M. *J. Solid State Chem.* **2006**, *179*, 3599.
(7) Lundgren, R. J.; Cranswick, L. M. D.; Bieringer, M. *Chem. Mater.* **2007**, *19*, 3945.
(8) Rao, C. N. R.; Raveau, B. *Transition Metal Oxides*; John Wiley & Sons: New York, 1988.
(9) Ranmohotti, K. G. S.; Josepha, E.; Choi, J.; Zhang, J.; Wiley, J. B. *Adv. Mater.* **2011**, *23*, 7309.
(10) Shafi, S. P.; Kotyk, M. W.; Cranswick, L. M. D.; Michaelis, V. K.; Kroeker, S.; Bieringer, M. *Inorg. Chem.* **2009**, *48*, 10553.
(11) Shafi, S. P.; Lundgren, R. J.; Cranswick, L. M. D.; Bieringer, M. *J. Solid State Chem.* **2007**, *180*, 3333.
(12) Ambrosini, A.; Duarte, A.; Poeppelmeier, K. R.; Lane, M.; Kannewurf, C. R.; Mason, T. O. *J. Solid State Chem.* **2000**, *153*, 41.
(13) Reid, A. F.; Sienko, M. J. *Inorg. Chem.* **1967**, *6*, 521.
(14) Kolitsch, U.; Tillmanns, E. *Acta Crystallogr.* **2003**, *E59*, i36.
(15) Rice, C. E.; Robinson, W. R. *J. Solid State Chem.* **1977**, *21*, 155.
(16) Rossell, H. J. *J. Solid State Chem.* **1976**, *19*, 103.
(17) Lyashenko, L. P.; Shcherbakova, L. G.; Belov, D. A.; Knotko, A. V. *Inorg. Mater.* **2009**, *45*, 543.
(18) Pokrovskii, B.; Isaeva, E. V. *Russ. J. Inorg. Chem.* **1977**, *22*, 1103.
(19) Knop, O.; Brisse, F.; Castelliz, L. *Can. J. Chem.* **1969**, *47*, 971.
(20) Brixner, L. H. *Inorg. Chem.* **1964**, *3*, 1065.
(21) Komissarova, L. N.; Shatskii, V. M. *Zh. Prikl. Khim.* **1966**, *39*, 2211.
(22) Goodenough, J. B. *Nature* **2000**, *404*, 821.
(23) Rodríguez-Carvajal, J. *FullProf. 2k*, Vers. 4.40; 2008.
(24) Hansen, T. C.; Henry, P. F.; Fischer, H. E.; Torregrossa, J.; Convert, P. *Meas. Sci. Technol.* **2008**, *19*, 034001.
(25) Wills, A. S. *VaList for Windows*, Vers. 1.5.8; 1998.